Electronic Supplementary Material (ESI) for Journal of Materials Chemistry C.

Supporting Information

Impact of Ultrathin Dielectric Spacers on SERS: Energy Transfer between Polarized Charges and Plasmons

*Deepak Ranjan Nayak, Navakanta Bhat, Murugesan Venkatapathi and Siva Umapathy**

COMPUTATION METHODS AND RESULTS

The COMSOL models used for calculation of the cross section is shown in the figures below.

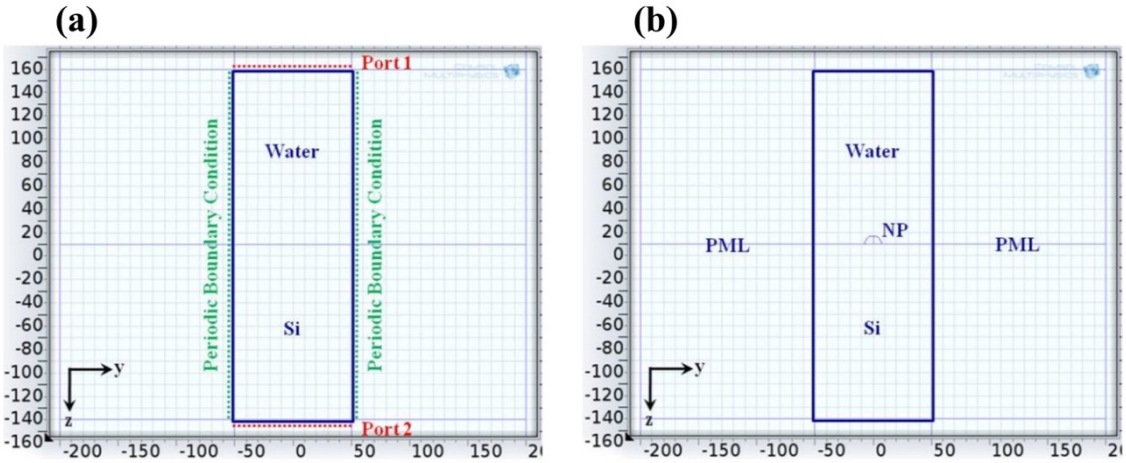

Figure S1. Simulation domain for (a) background EM field and (b) cross section calculation.

Following are the equations used for calculation of absorption cross section from resistive heating in COMSOL model.

$$CS_{abs} = \frac{\iiint P_{rh}\, dV}{\frac{1}{2} nc\varepsilon_0 E_0^2} \tag{1}$$

$$P_{rh} = \frac{1}{2} \vec{J} \cdot \vec{E} \tag{2}$$

The equations below are used for calculating scattering cross section from poynting vector and extinction cross section.

$$CS_{sc} = \frac{\iint n \cdot \vec{P}\, dS}{\frac{1}{2} nc\varepsilon_0 E_0^2} \tag{3}$$

$$CS_{ext} = CS_{abs} + CS_{sc} \tag{4}$$

For verification of the calculated cross section, the average electric field on the nanoparticle surface was calculated by port sweep and the peak positions of LSPRs were compared. Enhanced electric field (squared) is directly proportional to the cross section. The LSPR peaks obtained from both the simulation domain should match with minor variability.

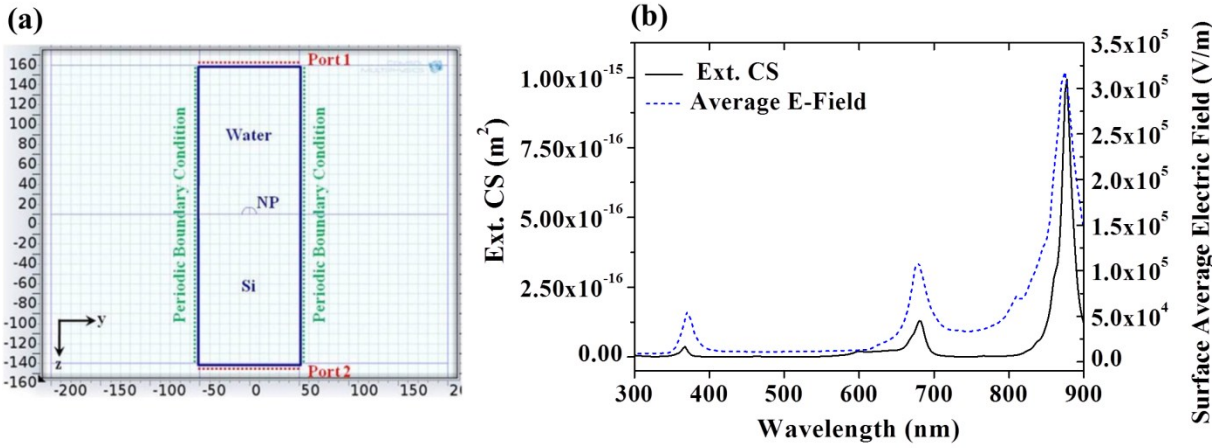

Figure S2. (a) Simulation domain to calculate the surface average electric field for nanoparticle on Si. (b) Comparison of Extinction cross section and electric field.

The equation used to calculate the surface average electric field on nanoparticle surface is,

$$E_{avg} = \frac{\iint \left(\sqrt{|E_x|^2 + |E_y|^2 + |E_z|^2}\right) ds}{Surface\ area} \tag{5}$$

Absorption cross section of 14 nm diameter Ag sphere and hemisphere in water is plotted in the figures below. This depicts the symmetry breaking in case of a hemisphere.

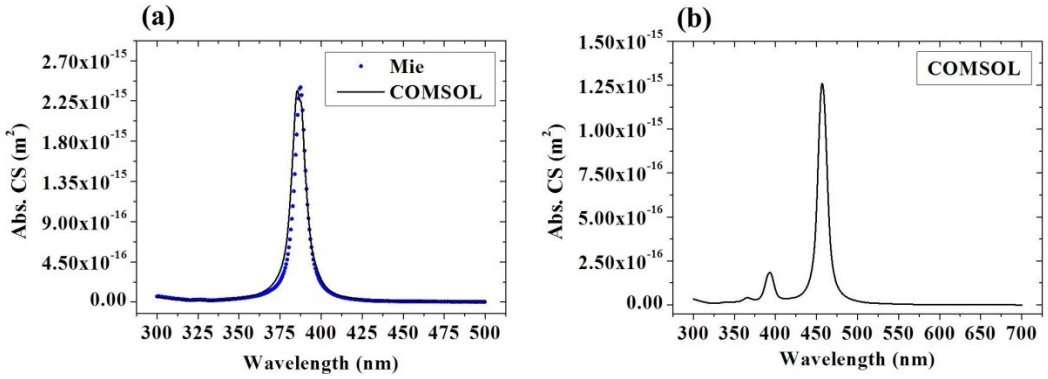

Figure S3. Absorption cross section of 14 nm (a)Ag sphere and (b) Ag hemisphere in water (COMSOL).

LSPR modes in Ag hemispheres and near field enhancements is shown below. The colour range of the figures has been adjusted for proper visualization of the enhancement regions on nanoparticle surface.

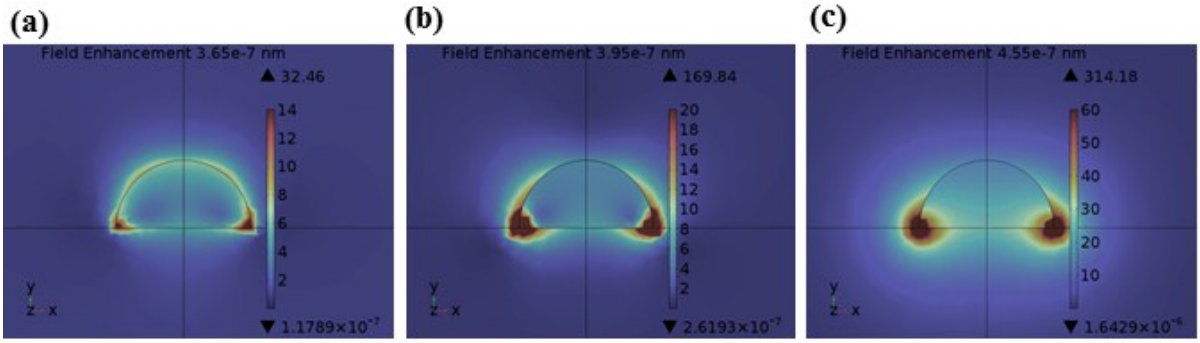

Figure S4. LSPR mode of Ag hemisphere in water at (a) 365 nm, (b) 395 nm and (c) 455 nm.

INTER-PARTICLE COUPLING

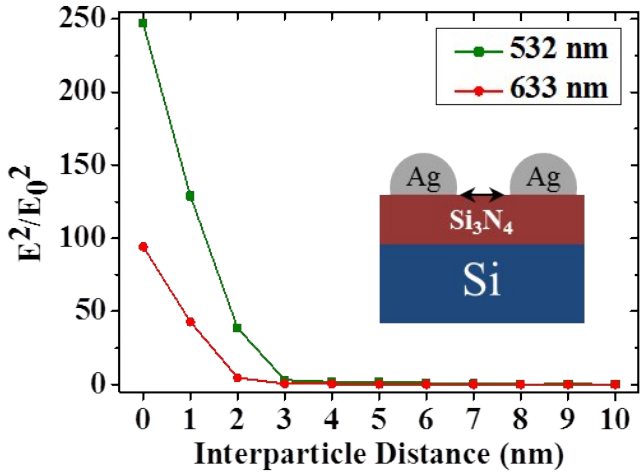

Figure S5. Inter-particle coupling strength on a substrate for 14 nm Ag nanoparticle.

EXTINCTION CROSS SECTION OF AGNP ON DIFFERENT SUBSTRATES

The figure below shows the extinction cross section of Ag hemisphere with diameter 10 nm, 12 nm and 14 nm on 5 nm films of SiO_2, HfO_2 and Si_3N_4. Red shift of LSPR peak with respect to permittivity of the film is observed.

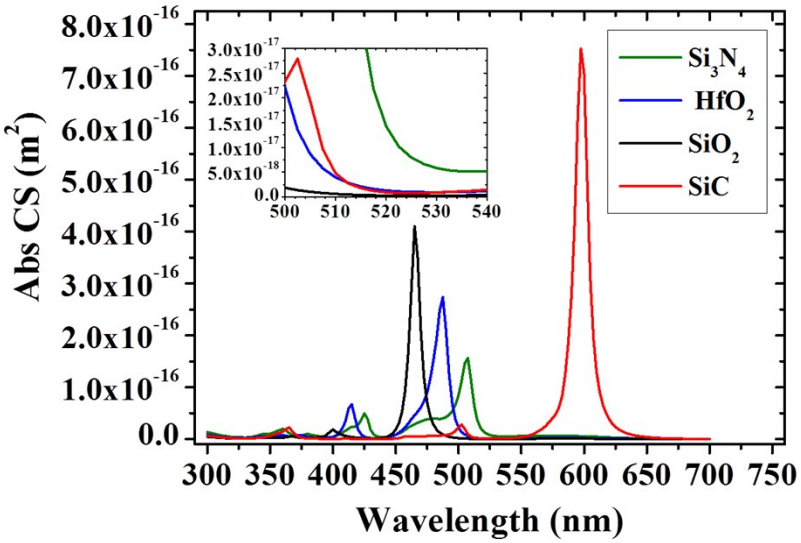

Figure S6. Extinction cross section of Ag hemisphere on different substrates. Inset graph shows the extent of resonance tail for different substrate.

There can be 2 reasons for the mismatch of the experiment and simulated results in Figure 5. The width of the LSPR will arise due to the broad distribution of the nanoparticle size. Hence, the computed LSPR of nanoparticle on substrate with SiO_2 and SiC may have a significant tail extending till 514 nm (inset image in Figure S6) which over estimated gain in case of Si_3N_4. Accurate prediction of LSPR position is also difficult, which resulted in over estimating the gain for Si_3N_4. The gains were calculated to be 94 and 82 by computation and analytical formula respectively.

The table below corresponds to the LSPR peak positions for hemisphere on different bulk substrates (without spacer).

Table S1. Estimated LSPR peaks.

LSPR Peak	Sphere	Hemi-sphere	Hemisphere on Bulk			
			SiO_2	Si_3N_4	SiC	Si

1st		366	370	361	363	367
2nd	387	393	403	438	497	661
3rd		457	476	533	590	863

PARTICLE VOLUME DENSITY

Table S2. Particle Volume per unit area for different substrates.

Films	Volume Density per unit area (nm^3/nm^2)
SiO_2	1.16
HfO_2	1
Si_3N_4	1.44
SiC	1.40

** the counts were taken for the size lying in the 1σ region*

OPTIMIZATION OF WIND MODEL

The figure below shows the comparison of the first LSPR peak position obtained from computation, original analytical formula by Wind *et.al.*, and our model.

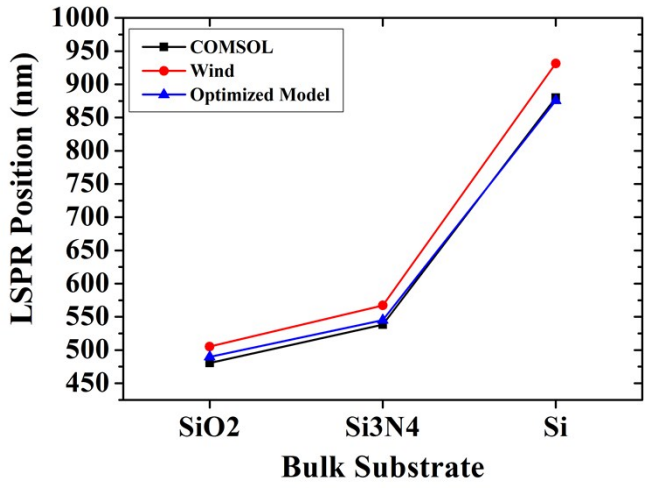

Figure S7. Comparison of LSPR peak calculated for bulk substrates.

ELLIPSOMETRY RESULTS

Standard Cauchy's model was used for fitting the parameters for different films. Standard database (JAP, 83 (1993), 3323) in the *Complete EASE, J.A. Woollam Co.* software was used for determining thermally grown SiO_2 thickness. The *Parameter Uniqueness Fit* and the *Correlation matrix* should be analyzed to verify the thickness value. An example is given in Figure S8 to compare a best fit model with two misfit models. The model in Figure S8 (a) has the thickness uniqueness at 5.39 nm with least MSE and (b) at 6.15 nm. It is important to note that the least MSE for (b) is at 6.15 nm but for the range of thickness 4.5 nm-6.5 nm the MSE does not change significantly. Hence it is difficult to estimate the thickness of film which is anywhere between 4.5 nm-6.5 nm. But the dataset at (a) has a unique thickness and hence this model is reliable. The model in Figure S8 (c) is erroneous compared to other two. Similar cautions were taken to obtain the thickness and optical constants for other thin films.

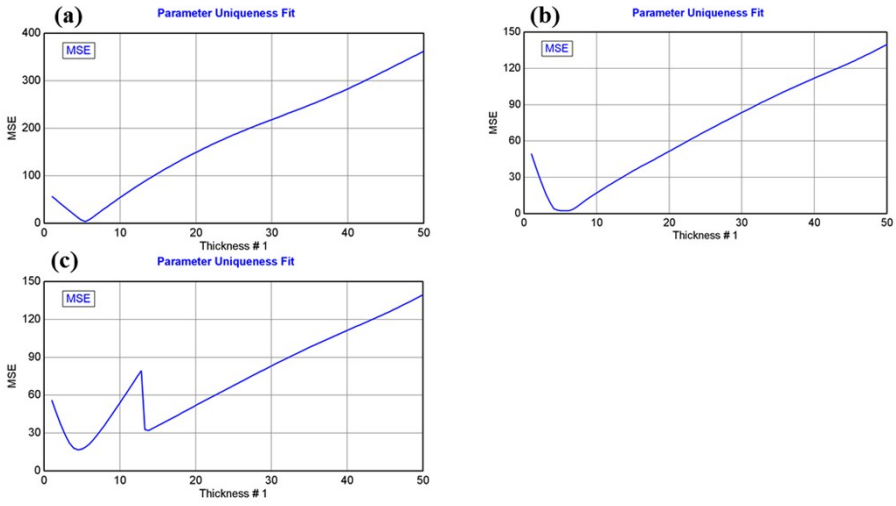

Figure S8. Comparison of *Parameter Uniqueness Fit* for 5 nm SiO_2 for different models.

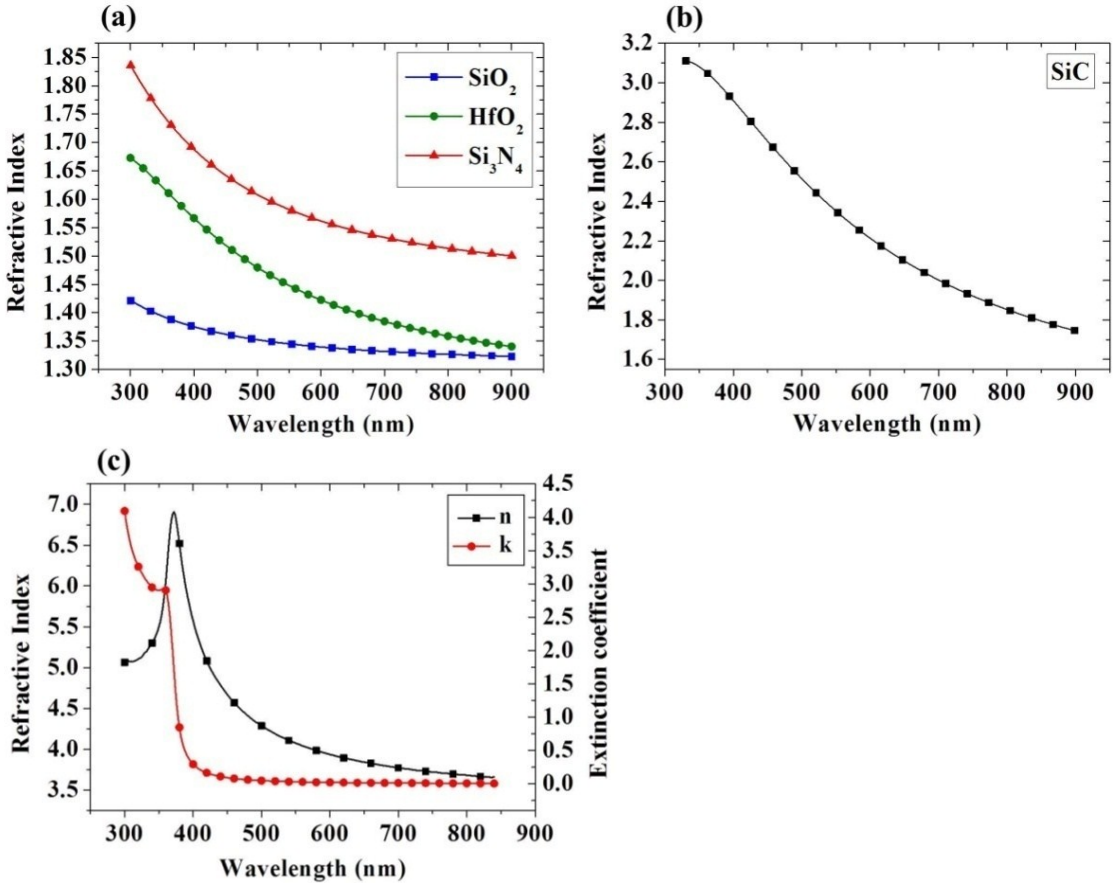

Figure S9. Experimental permittivity of 5 nm film of a) SiO_2, HfO_2, Si_3N_4 and b) SiC. c) n and k value of bulk Si <100>.

We have also carried out HR SEM with Zeiss ULTRA 55 equipped with Gemini Column, which has capability of reaching sub-nanometer resolution. One of such images is provided below for a 5 nm LPCVD Si_3N_4film on Si with Ag nanoparticle.

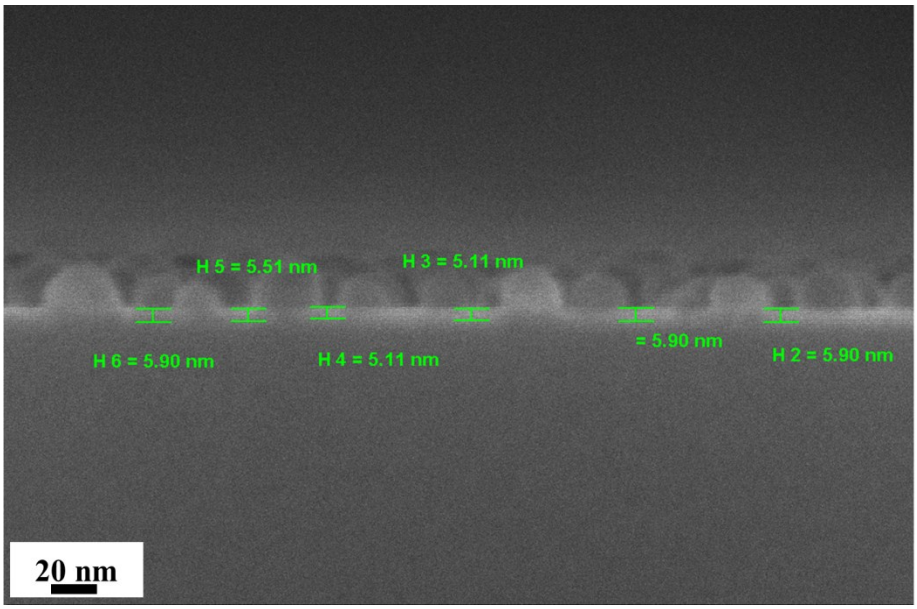

Figure S 10. High resolution SEM image of 5 nm Si_3N_4 film on Si.

As discussed earlier, the Ellipsometry results were carefully analyzed to obtain the permittivity as well as the thickness values. The thickness for the above film was found to be 5.44 nm±0.066 nm through ellipsometry.

Table S3. Refractive index of films at different wavelengths.

Films	@514 nm	@ 532 nm	@ 633 nm
SiO_2	1.35	1.35	1.33
HfO_2	1.47	1.46	1.40
Si_3N_4	1.60	1.59	1.55
SiC	2.46	2.41	2.14

NORMAL RAMAN SPECTRA AND PEAK ASSIGNMENT

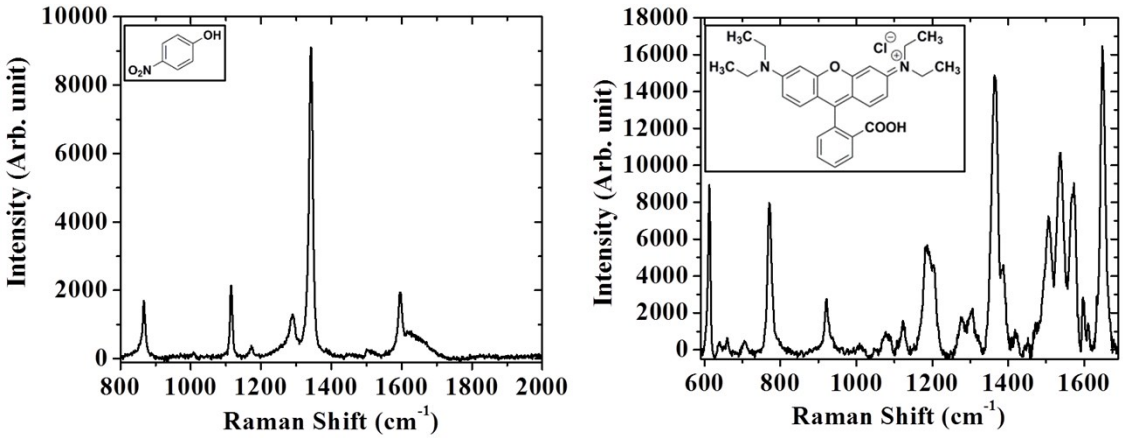

Figure S11. NR spectrum of a) PNP and b) R6G.

The peak assignments of different modes of R6G and PNP are given below.

Table S4. Peak assignment for PNP.

Wavenumber (cm^{-1})	Assignment
819	NO_2 bend
859, 951	C-H out-of-plane bend
1078	ring CCC bend
1116	C-H in-plane bending motion
1245	C–H bend (in-plane)/NO_2 asym. stretch
1320	C–H bend (in-plane) /NO_2 symm. stretch
1592	ring deformation

Table S5. Peak assignment for R6G.

Wavenumber (cm^{-1})	Assignment
612, 664, 702	in-plane xanthene ring deformation
774	out-of-plane C-H bend
1084, 1122	in-plane C-H bend
1181	in-plane xanthene ring deformation, C-H bend, N-H bend
1268	C-O-C stretch
1310	in-plane xanthene ring breath, N-H bend, CH_2 wag
1362	xanthene ring stretch, in-plane C-H bend
1507, 1535	aromatic C-C stretch
1576	xanthene ring stretch, in-plane N-H bend
1599, 1606	aromatic C-C stretch
1650	xanthene ring stretch, in-plane C-H bend

COMMENTS ON ACCURACY OF ENHANCEMENT MECHANISM

Effect of nanoparticle distribution on enhancement factors

Varying thickness of the films does not result in the change in the nanoparticle size largely, and the cross-sections (dominated by absorption) are only a function of volume deposited per area which is nearly constant for all spacers. Other experiments and models have been reported elsewhere with varying thickness i.e. in the non-radiative regime (10-40 nm) where these effects are monotonic, and in the radiative regime (> 40nm) where the spacer effect is oscillatory.

The NP size is extremely small to contribute to scattering and hence absorption is the most important factor modulating the plasmon response. Absorption is dependent on surface density of metal particles (volume per unit area), which is kept nearly constant for all substrates.

The size distribution will result in the redshift of the LSPR peak as well as variation in the absorption cross section in a specific substrate. These have been incorporated in the model through equations 5 (shift) and 6 (amplitude) and the measured size distributions. Given that the size of the nanoparticles is extremely small, the increase in size does not result in any notable changes as the volume of metal particles is nearly conserved for all films, even though our calculations does include effects of size dispersion.

To further support this claim, the extinction cross section plot of AgNP on substrate with Si_3N_4 spacer has been given below.

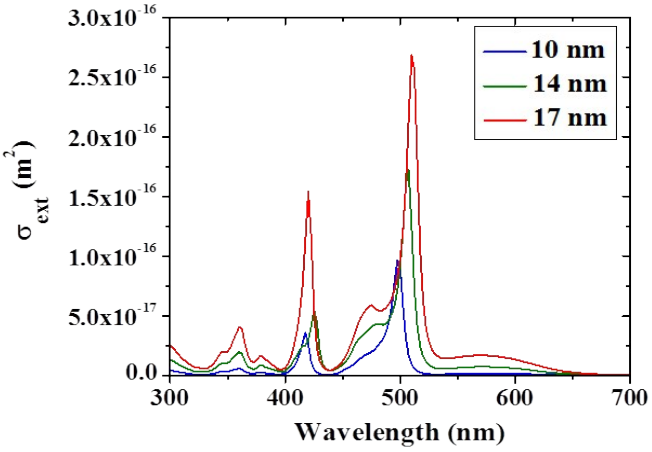

The distribution in Fig 1a suggests NP size variation from 10 nm-17 nm. The σ_{ext} (Extinction Cross section) plot shows LSPR shift of 12 nm with magnitude of 2.7 times increment for 10 nm

to 14 nm NP size increment. This effect will further subside when the relative gains are plotted with respect to a specific substrate.

Limitations in direct observation of LSPR experimentally

There are experimental limitations in observing LSPR directly for very small nanoparticles and the reason is two folds.

Techniques, such as cathodoluminescence and dark-field microscopy, are scattering based measurements and intensity varies as the typical cross section expression with a^6 (a being the diameter). Direct measurement of LSPR involving small nanoparticles with diameter less than 50 nm is challenging.

The complexity of the experiment further increases especially on substrates which are not transparent i.e. the absorption by metal particles cannot be estimated using transmission through substrate. One of the authors' report[†] suggest that the measurements with dark-field microscopy is very specific to the substrate property. Gold nanoparticles (<~200 nm diameter) were observed only on specific substrates and smaller NPs were not visible.

[†]*Chakraborty, Krishnendu, et al. "Enhancement of scattering from nanoparticles using substrate effect."SPIE BiOS.International Society for Optics and Photonics, 2016.*